Journal of the Optical Society of Korea
Vol. 17, No. 5, October 2013, pp. 433-440
DOI: http://dx.doi.org/10.3807/JOSK.2013.17.5.433

Evaluation of Chromatic-Dispersion-Dependent Four-Wave-Mixing Efficiency in Hydrogenated Amorphous Silicon Waveguides

Dong Wook Kim[1], Heung Sun Jeong[1], Sang Chul Jeon[2], Sang Hyun Park[2], Dong Eun Yoo[2], Ki Nam Kim[2], Shin Mo An[3], El-Hang Lee[3], and Kyong Hon Kim[1]*

[1]*Department of Physics, Inha University, Incheon 402-751, Korea*
[2]*National Nanofab Center, 335 Gwahangno, Yuseong-gu, Daejeon 305-806, Korea*
[3]*Graduate School of Information Technology, Inha University, Incheon 402-751, Korea*

(Received August 2, 2013 : revised September 27, 2013 : accepted September 30, 2013)

We present an experimental and numerical study of spectral profiles of effective group indices of hydrogenated amorphous silicon (a-Si:H) waveguides and of their chromatic-dispersion effect on the four-wave-mixing (FWM) signal generation. The a-Si:H waveguides of 220-nm thickness and three different widths of 400, 450 and 500 nm were fabricated by using the conventional CMOS device processes on a 2-μm thick SiO_2 bottom layer deposited on 8-inch Si wafers. Mach-Zehnder interferometers (MZIs) were formed with the a-Si:H waveguides, and used for precise measurement of the effective group indices and thus for determination of the spectral profile of the waveguides' chromatic dispersion. The wavelength ranges for the FWM-signal generation were about 45, 75 and 55 nm for the 400-, 450- and 500-nm-wide waveguides, respectively, at the pump wavelength of 1532 nm. A widest wavelength range for the efficient FWM process was observed with the 450-nm-wide waveguide having a zero-dispersion near the pump wavelength.

Keywords : Silicon photonics, Nonlinear optic waveguide, Four-wave-mixing
OCIS codes : (190.4380) Nonlinear optics, four-wave-mixing; (230.7370) Waveguides

I. INTRODUCTION

Recently hydrogenated amorphous silicon (a-Si:H) waveguides have attracted significant interest for their potential applications to nonlinear optic devices because the a-Si:H material has a relatively high-nonlinear-optic property compared to the crystalline silicon, and can be easily obtained for device fabrication with the complementary metal-oxide-semiconductor (CMOS) device process [1-3]. While the conventional silicon waveguides are formed on the silicon-on-insulator (SOI) wafers which are produced through a delicate wafer-bonding process, the a-Si:H waveguides can be formed on an a-Si:H layer which is deposited directly on the conventional silicon wafer with using a plasma-enhanced chemical vapor deposition (PECVD) process after a silicon-dioxide (SiO_2) bottom layer deposition. Furthermore, the amorphous silicon can be formed in the multi-stacked layers, thus offering much freedom for complex device fabrication. Recent technological development has shown a significant reduction of the optical loss which is comparable to that of the single-crystal silicon. In addition, the a-Si:H waveguides have been used for photon pair generation through the four-wave-mixing (FWM) process [4, 5].

Nonlinear optic devices, especially correlated photon-pair generation devices based on the FWM process, require not only low optical-loss of the a-Si:H material but also the optimized chromatic-dispersion (CD) property of the waveguides [2, 6]. The CD property affects the phase-matching condition among the pump, signal and idler beams in the FWM process, and thus influences the efficiency of the FWM-beam generation. The CD properties of nano-scale waveguides have been analyzed extensively for the crystalline silicon [7-12], and it has been known that their CD properties depend significantly on waveguide size even for the same core and clad material structure. The core-dimension-dependent CD properties and nonlinear effect of the crystalline silicon

*Corresponding author: kyongh@inha.ac.kr
Color versions of one or more of the figures in this paper are available online.

waveguides have been investigated in the previous reports. However, no detailed analysis on the CD properties and nonlinear effect of the a-Si:H waveguides has been reported yet.

In this paper we report on the experimentally measured CD properties of the a-Si:H waveguides of 220-nm thickness having three different widths of 400, 450 and 500 nm, and on their comparison with numerically simulated results. We also present their effect on the FWM-signal-generation efficiency based on experimentally measured and numerically calculated results.

II. WAVEGUIDE DESIGN AND FABRICATION

The spectral profile of the refractive index of the a-Si:H material was measured with an ellipsometer after a thin film deposition with the PECVD process on the top of a SiO_2 layer which was also formed directly on a silicon wafer. The a-Si:H film was deposited at a gas-mixing condition of 1:15 ratio of a precursor gas Silane (SiH_4) and a hydrogen gas (H_2), at the total gas pressure of 2.0 torr, at an RF power of 100 W, and at a substrate temperature of 300℃. Figure 1 shows a refractive-index profile of the a-Si:H layer measured by using the ellipsometric method and compared with the known refractive-index values of the a-Si:H material [13]. The measured refractive index of the a-Si:H layer at the He-Ne laser wavelength of 632.8 nm was 4.0423. By comparing this value with the data reported by R.J. Severens *et al* [14], the hydrogen concentration in this a-Si:H layer is determined to be about 720×10^{19} cm^{-3} which corresponds to 14.4 atomic %.

Three types of the a-Si:H waveguide with a fixed height of 220 nm but with three different widths of 400, 450 and 500 nm were designed and fabricated. Before fabrication of the a-Si:H waveguides, the SiO_2 layer was first deposited into a 2-μm thickness at a temperature of 400℃ on a 750-μm-thick silicon wafer as a bottom-cladding layer using the PECVD process. Then, a chemical-mechanical-polishing (CMP) process was performed to achieve a smooth top surface of the SiO_2 layer up to the root-mean-square (RMS) surface roughness of about 0.4 nm as it was measured by an atomic-force microscope (AFM) within a 5-μm×5-μm area. In the next step, a 220-nm-thick a-Si:H layer was deposited on the SiO_2 film by using the PECVD method. Electron-beam-lithography and dry-etching processes were then applied to fabricate waveguide patterns on the a-Si:H layer. The fabricated a-Si:H waveguides had the same 220-nm height but three different widths of 400, 450 and 500 nm. The waveguides had 200-μm-long inverse-tapered-coupling sections at both ends with a 100-nm-wide-end cross section. The a-Si:H layer was covered with a SiO_2-layer upper cladding. Integrated Mach-Zehnder-interferometer (MZI) devices with two arms of asymmetric lengths were also fabricated with each of the three different-thickness waveguides for measurement of each group index.

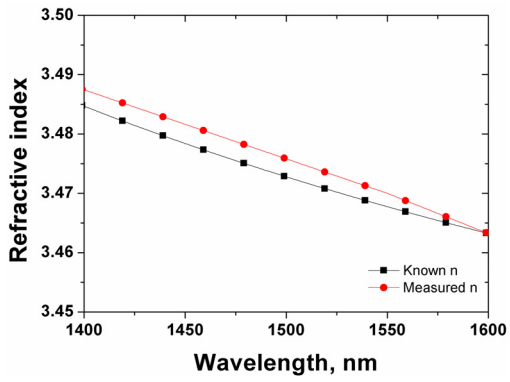

FIG. 1. Measured refractive-index profile of the a-Si:H film compared with the known values [13].

The effective refractive indices of the waveguides for light-beam propagation of transverse-electric (TE) and transverse-magnetic (TM) modes were calculated by using a commercial software based on the finite-element method (Rsoft FEMSIM), and were used for calculation of the CD values. The calculated TE-mode profile in the a-Si:H waveguide of a 220-nm×450-nm cross-section embedded in the SiO_2 material is shown in Fig. 2(a). The calculated

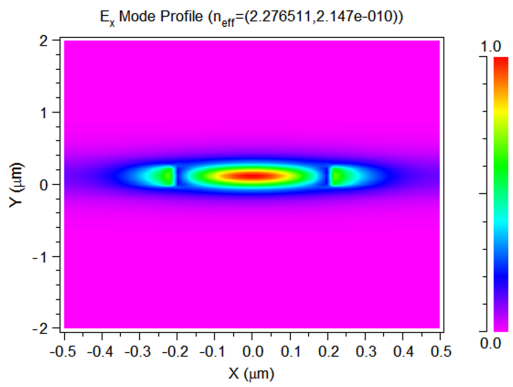

(a)

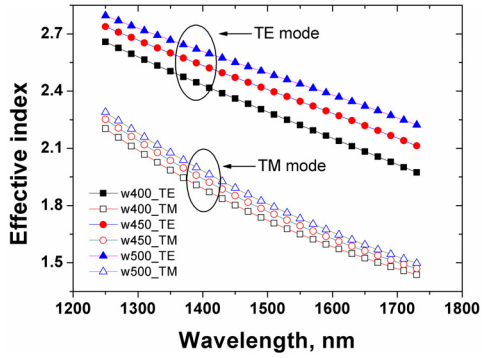

(b)

FIG. 2. (a) Mode profile of an a-Si:H waveguide with a 220×450-nm cross-section for the fundamental TE-mode, and (b) calculated effective indices of the waveguides of 220-nm height and of three-different widths. Filled symbols are for the TE-mode, and open symbols are for the TM-mode.

effective-index profiles of the three different waveguide widths are plotted in Fig. 2(b). In this calculation, the Sellmeier equation of the silica (SiO_2) material [15] and the measured refractive-index profile of the PECVD-deposited amorphous silicon were used. The calculated effective indices of the TE mode are larger than those of the TM modes. Based on these effective-index values of the waveguides, the group indices and CD values were obtained, and compared with the measured results, as discussed in the next section.

III. EXPERIMENTAL RESULTS

3.1. Group Index Measurement and Chromatic Dispersion Determination

The group-index (GI) profiles of the fabricated a-Si:H waveguides were determined by measuring the interference-spectrum output of the MZIs under illumination of an amplified super-luminescent diode (SLD) at the 1.5-μm -wavelength range with an erbium-doped-fiber amplifier (EDFA). The polarization of the amplified-SLD output was adjusted with a polarization controller (PC), and selected to either one of the waveguide TE and TM modes with a fiber-type polarization-beam-splitter (PBS) of a 30-dB extinction ratio. The light was launched into and collected from the inversely tapered ends of the a-Si:H waveguide by using tapered polarization-maintaining-fibers (PMFs) at both ends. The transmitted output beam of the MZIs was measured by an optical spectrum analyzer (OSA) with a 70-pm resolution.

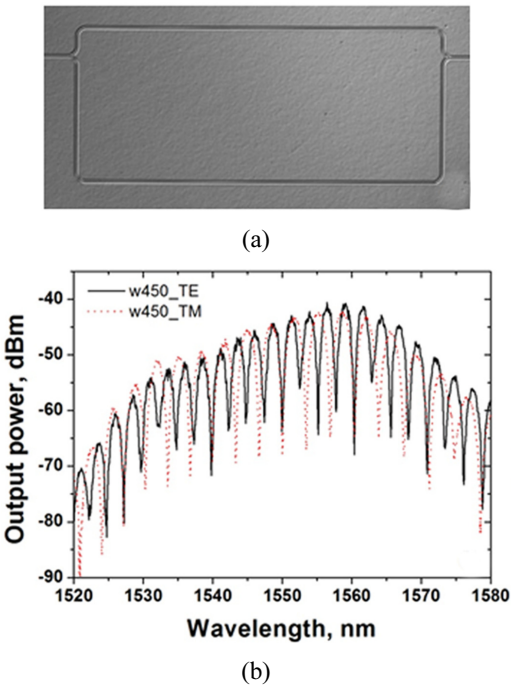

(a)

(b)

FIG. 3. (a) Optical microscope image of the fabricated MZI with the 220 nm×450 nm a-Si:H waveguide and (b) measured output spectra of the MZI. Black solid line and red dotted line are for each of the TE and TM modes, respectively.

Figure 3(a) shows an optical microscope image of the fabricated MZI with the 220-nm×450-nm a-Si:H waveguide. The MZI was formed with two Y-branches and with a path-length-difference of 200 μm between two arms. The bending radius of the Y-branches was about 5 μm. It is known that, as long as the bending radius was larger than 2 μm, optical loss at the bending region was negligible, and waveguide-dispersion impact was minimal. From the path-length difference between two arms, a relative phase-shift occurred between two light outputs passing through the arms. As a result, the interference fringes at the output of the MZI were measured. The measured spectral-interference output of the MZI is shown in Fig 3(b). Measured extinction ratios of the MZI-interference spectra were about 20 dB and 25 dB for TE and TM modes, respectively. Since the relative phase-difference between a peak and its adjacent minimum valley was equal to π, the group-index profile of the a-Si:H waveguide can be determined from the interference fringe according to the theoretical relationship between the group index and the interference fringe [16, 17]:

$$n_g \cong \frac{\lambda_{\max}\lambda_{\min}}{2\Delta L\Delta\lambda} \tag{1}$$

where λ_{max} and λ_{min} are the maximum and minimum peak wavelengths, respectively. ΔL is the length difference between the two arms, and $\Delta\lambda$ is wavelength difference between a peak and its adjacent minimum valley.

Figures 4 (a) and (b) show the measured group-index profiles of the a-Si:H waveguides for the TE and TM modes, respectively, obtained from the measured interference fringes. Each plot with a different symbol represents the measured group-index values for each of the waveguides of three different widths. The line curves indicate the calculated group-indices based on the spectral effective-index profiles shown in Fig. 2(b). The group index can be calculated from the effective refractive-indices using the following relationship [14].

$$n_g = n_{eff} - \lambda\frac{dn_{eff}}{d\lambda} \tag{2}$$

The plots indicate that the measured group index n_g values of the TE-mode beam from the MZI interference spectrum matches well with the calculated values from the effective index n_{eff} although the measured data show some fluctuation. However, the measured group index n_g values of the TM-mode beam from the MZI interference spectrum shows significant data fluctuations. Thus, the measured group index n_g values of the TM-mode beam are not useful for further analysis. There is an inflection point in

the spectral group-index profiles of the 450- and 500-nm-wide waveguides within the wavelength range from 1500 nm to 1600 nm for the TE-mode. This means that the sign of the $dn_{eff}/d\lambda$ term changes around the inflection-point wavelength. Since the chromatic-dispersion parameter D is expressed, from [15], as

$$D = \frac{1}{c}\frac{dn_g}{d\lambda} = -\frac{\lambda^2}{2\pi c}\left|\frac{d^2\beta}{d\lambda^2}\right| \quad (3)$$

where c is the speed of light in free space. $dn_g/d\lambda$ is zero at the infection point, the CD value at the inflection-point wavelength is zero. The calculated zero-dispersion-wavelengths (ZDWs) of the three different waveguides of 400-, 450- and 500-nm widths were about 1590, 1518 and 1509 nm, respectively.

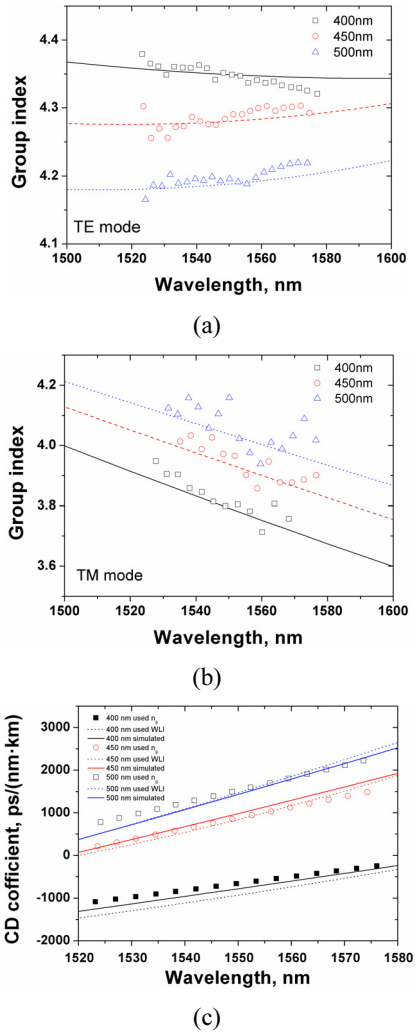

FIG. 4. Measured group-index profiles of the waveguides for (a) TE and (b) TM modes. Symbols represent measured n_g values and the lines indicate the calculated results with Eq. (2) and Fig. 2(b). (c) Comparative plots of measured (symbols) and calculated (solid lines) CD-profiles of the a-Si:H waveguides of three different-widths for the TE-mode. Dotted lines are the measured CD-profiles using the white-light-interferometer method.

The CD values of the waveguides was measured experimentally by using a white-light interferometer (WLI) method [11] and also determined from the measured group index profiles. Spectral profile of the phase changes in the interference spectra of the WLI outputs was measured when a reference sample placed in one arm of the WLI was replaced with an a-Si:H-waveguide sample, and used to determine the precision CD values of the sample. The obtained CD coefficients of the a-Si:H waveguides of three different widths are plotted in Fig. 4(c) with symbols indicating the data obtained from the measured group index values, with solid lines corresponding to the experimental results measured using the WLI method, and with dotted lines representing numerical results calculated from the n_{eff} -based n_g lines of Figs. 4(a) and (b). The measured ZDWs were about 1596, 1520 and 1503 nm, respectively, for the waveguides of 400-, 450- and 500-nm widths. Both measured and calculated results are very close to each other. The results indicate that validity of our numerical and experimental approaches determining the CD values based on the effective-index calculation and the WLI measurement method is supported by the CD values obtained from the group-index values measured directly with the MZI patterns which are composed of the same-type waveguides. For the FWM generation efficiency analysis, we use the CD values measured with this WLI method.

3.2. Four-wave-mixing Process in a-Si:H Waveguides

The experimental setup used for the FWM measurement is illustrated in Fig. 5. Two tunable lasers were used as pump and signal beam sources for the FWM experiment with the a-Si:H waveguides. The pump wavelength was fixed at 1532 nm while the signal wavelength was swept from 1520 to 1570 nm. The tunable-laser-source signals were amplified with high-power erbium-doped-fiber amplifiers (EDFAs). After amplification through the high-power EDFAs, the ASE noises from the amplified pump- and signal-beams were filtered out with narrow band-pass filters. The polarizations of the pump- and signal-lightwaves were aligned

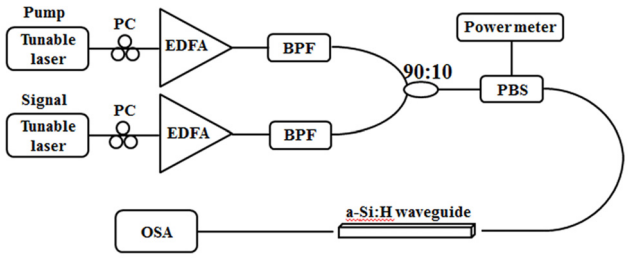

FIG. 5. Experimental setup used for measuring the FWM effect in the a-Si:H wavaguides. (PC: polarization controller, EDFA: erbium doped fiber amplifier, BPF: band-pass filter, PBS: polarization beam splitter, OSA: optical spectrum analyzer)

to the same TE-polarization direction of the waveguide with PCs and a fiber-type PBS. Then, the two lightwaves were combined with a 90:10 coupler, and their TE-polarization beams were inputted into the a-Si:H waveguide in its TE-mode direction via the PBC and a tapered PM fiber. The optical output from the a-Si:H waveguide was measured with an optical spectrum analyzer (OSA). Three different a-Si:H waveguides with cross-section sizes of 220-nm height and of 400-nm, 450-nm and 500-nm widths but all with the same waveguide length of 6 mm were used for the FWM-signal-conversion-efficiency measurement. Propagation losses of the three waveguides were about 0.67, 0.55 and 0.45 dB/mm, respectively, for the TE-mode. Our a-Si:H waveguides had higher propagation losses than others reported in Refs. 4 and 5. This might be attributed to non-optimized sidewall roughness of our waveguides. The fiber coupling loss to the inverse tapered waveguide end was about 11 dB/facet for the TE-mode beam input.

The signal-idler generation efficiency through the degenerated FWM process can be analyzed with the coupled-mode equations [18, 19]:

$$\frac{dP_p}{dz} = -\alpha P_p - 4\gamma\sqrt{P_p^2 P_s P_i}\sin\theta \tag{4}$$

$$\frac{dP_s}{dz} = -\alpha P_s + 2\gamma\sqrt{P_p^2 P_s P_i}\sin\theta \tag{5}$$

$$\frac{dP_i}{dz} = -\alpha P_i + 2\gamma\sqrt{P_p^2 P_s P_i}\sin\theta \tag{6}$$

$$\frac{d\theta}{dz} = \Delta\beta + \gamma(2P_p - P_s - P_i) + \gamma[\sqrt{P_p^2 P_i / P_s} + \sqrt{P_p^2 P_s / P_i} - 4\sqrt{P_i P_s}]\cos\theta \tag{7}$$

where α is the absorption coefficient of the a-Si:H waveguide per unit length. $\gamma = 2\pi n_2/\lambda A_{eff}$ is the nonlinear coefficient of the waveguide, A_{eff} is the effective core area of the waveguide cross-section. λ is the light wavelength in free space, and n_2 is the nonlinear refractive index of the optical waveguide material. P_p, P_s, and P_i are pump, signal, and idler beam powers, respectively. $\Delta\beta$ represents the linear phase-mismatch among the signal, pump and idler beams in the degenerated FWM process, and it should be zero to satisfy the phase-matching condition:

$$\Delta\beta = \beta(\omega_s) + \beta(\omega_i) - 2\beta(\omega_p) = 0 \tag{8}$$

where $\beta(\omega_{s,i,p})$ represent the propagation constants of the signal, idler and pump beams, respectively, at their angular frequencies $\omega_{s,i,p}$.

If we expand the wave propagation constant using Taylor series about a reference frequency (i.e. a reference wavelength) $\omega_0 = 2\pi c/\lambda_0$, it can be written as

$$\beta(\omega) = \beta(\omega_0) + (\omega-\omega_0)\left|\frac{d\beta}{d\omega}\right| + \frac{1}{2}(\omega-\omega_0)^2\left|\frac{d^2\beta}{d\omega^2}\right| + \frac{1}{6}(\omega-\omega_0)^3\left|\frac{d^3\beta}{d\omega^3}\right| + ... \tag{9}$$

From Eqs. (3), (8) and (9), the linear phase-mismatch $\Delta\beta$ can be rewritten, in terms of the frequency f ($=\omega/2\pi = c/\lambda$), as

$$\Delta\beta = \frac{\pi\lambda_0^2 D_c(\lambda_0)}{c}\left[\frac{2\lambda_0}{3c}\{(f_s-f_0)^3 + (f_i-f_0)^3 - 2(f_p-f_0)^3\} - \{(f_s-f_0)^2 + (f_i-f_0)^2 - 2(f_p-f_s)^2\}\right] + \frac{\pi\lambda_0^4}{3c^2}\left[\frac{dD_c(\lambda)}{d\lambda}\right]_{\lambda=\lambda_0}\{(f_s-f_0)^3 + (f_i-f_0)^3 - 2(f_p-f_0)^3\}. \tag{10}$$

where $[dD_c(\lambda)/d\lambda]_{\lambda=\lambda_0}$ is dispersion slope at the reference wavelength λ_0 ($= c/f_0$).

The FWM-signal-conversion efficiency is defined as

$$G_i = \frac{P_{idler}(L)}{P_{signal}(0)} \tag{11}$$

where $P_{idler}(L)$ is the generated idler-beam power after propagation over the waveguide length L, and $P_{signal}(0)$ is the coupled input-signal-power to the waveguide.

The FWM-signal-conversion efficiency was calculated with an assumption that the coupling losses of the signal beam both at the output and input coupling sections were the same and the idler beam had the same coupling loss at the output coupling section. The coupling loss and waveguide

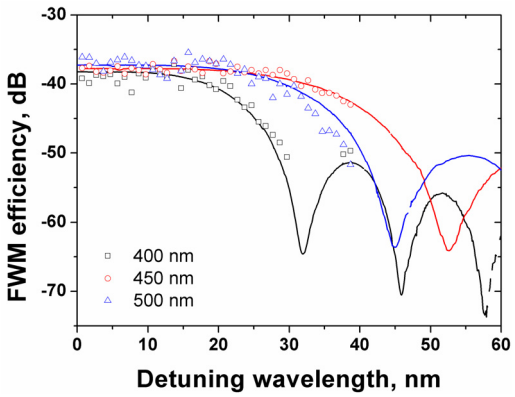

FIG. 6. FWM conversion efficiencies for the TE-mode-beam input in the three waveguides measured and calculated as functions of the signal wavelength at a fixed pump-wavelength of 1532 nm. Symbols and solid lines represent measured and calculated FWM efficiencies, respectively. The error ranges for the measured data were within 1~3 dB.

loss were determined by using the same-type a-Si:H waveguides of various lengths as described in Ref. 11. Then, the input signal power $P_{signal}(0)$ was determined at the beginning of the plane strip channel waveguide section by accounting the coupling loss of the input signal beam at the input coupling section. The idler beam power at the end of the plane strip channel waveguide section right after the inversely tapered coupling section $P_{idler}(L)$ just before the inversely tapered output fiber coupling section was also determined by accounting the coupling loss of the measured output idler beam power at the output coupling section. Then, the FWM efficiency was calculated by using Eq. (11).

The measured FWM-signal-conversion efficiencies of the 400-, 450- and 500-nm-wide a-Si:H waveguides with a fixed pump-beam of 1532-nm wavelength are shown in Fig. 6 with marks of open squares, circles, and triangles, respectively, and compared with the calculated ones from the coupled-mode equations in Eqs. (4) to (7). As shown in Fig. 4(c), the two waveguides of 450-nm and 500-nm widths have the anomalous GVD at wavelengths around 1530 nm, and have wider wavelength ranges for an efficient FWM process than the 400-nm-wide waveguide does. For these measurements, the coupled pump-power was fixed to +13 dBm.

The wavelength range of the 3-dB-drop FWM-beam generation efficiency from the peak value covers about 42, 75 and 65 nm for the 400-, 450- and 500-nm-wide waveguides, respectively. Since the zero-dispersion wavelength of the 220-nm×450-nm waveguide is close to the pump wavelength of 1532 nm, the signal light can be tuned in a wide wavelength-range for relatively high FWM-beam-generation efficiencies compared to the other size waveguides. It is expected that the FWM-beam-generation bandwidth will be extended over 100 nm if the pump wavelength is tuned close to the zero-dispersion wavelength.

The measured FWM-beam-generation efficiencies for various coupled-pump-powers at 1532 nm in the TE-polarization-mode of the 220-nm×450-nm waveguide are plotted with symbolic marks in Fig. 7. The calculated FWM efficiencies are also plotted in the same figure. The FWM efficiency was -35 dB at the coupled pump-power of +13 dBm, and decreased as the coupled pump power was reduced. The full wavelength range for the efficient FWM-beam-generation could not be measured experimentally due to the limited-wavelength coverage of our experimental equipments. The inset in Fig. 7 shows the measured FWM spectrum with the 1532-nm-pump and 1543-nm-signal beam wavelengths.

The nonlinear refractive index of the a-Si:H material was determined by varying the n_2 value in the nonlinear coefficient of the waveguide γ for the coupled-mode equations (4)~(7) and by comparing the calculated FWM efficiency with the measured results as shown in Fig. 7. The best fitting value of n_2 from the comparison between the calculated and measured results turns out to be $(1.17\pm0.52) \times 10^{-17}$ m^2/W, which is comparable to previously reported values in Refs. 1, 2, 20 and 21. This n_2 value is about 5 times larger than that of the crystalline silicon.

Figure 8 shows the measured and the calculated FWM-beam-generation efficiencies of the 220-nm x 450-nm waveguide as a function of the coupled pump-power at 1532-nm wavelength. In the logarithmic scale of both x- and y-axes, the FWM efficiency is almost linear with the pump power in a range from +3 to +13 dBm. The FWM-efficiencies calculated numerically by using Eqs. (4) to (7) match well with the measured results within the experimental error bars, which correspond to the standard deviations from the mean values of five measurement runs at each coupled pump-power. Our measured FWM conversion

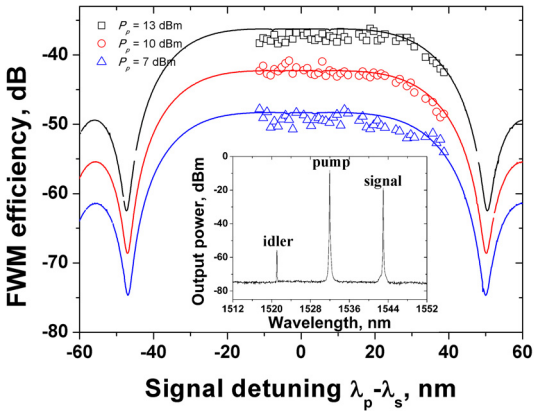

FIG. 7. FWM conversion efficiencies measured with the 220 nm×450 nm a-Si:H waveguide for the TE-mode beam input under three different pump powers of 13, 10 and 7 dBm. Symbols represent the measured FWM efficiencies, and solid lines indicate the calculated results. Inset shows the measured FWM spectrum at 1532-nm-pump wavelength.

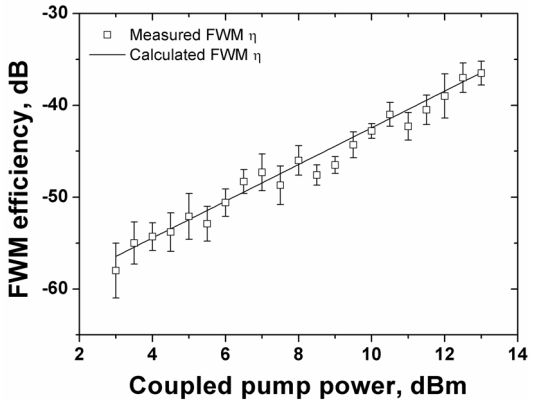

FIG. 8. Measured and calculated FWM-efficiencies as functions of the coupled pump power. Squares represent the measured FWM-efficiencies with error bars, and the solid line indicates the calculated results using the Eqs. (4) to (7). The error bars indicate the standard deviations from the mean values of five measurement runs at each coupled pump-power.

efficiencies are a little lower than those reported in Ref. 1 probably due to a relatively high waveguide loss of our sample compared to the other's. A further improvement can be made by having a uniform material property of the a-Si:H layer and smooth surfaces via a fine vertical-side wall etching.

IV. CONCLUSION

In this paper, we have presented experimentally-measured and numerically-calculated results of the chromatic-dispersion-dependent FWM-beam-generation efficiencies of three different a-Si:H waveguides of 400-, 450- and 500-nm widths but of a fixed 220-nm height. The effective group indices of the three different a-Si:H waveguides were determined by fabricating integrated Mach-Zehnder interferometer (MZI) devices of asymmetric arm lengths with the a-Si:H waveguides and by measuring their interference-spectrum outputs, and compared with the numerically calculated values from the effective refractive indices of the waveguides which were obtained with the Sellmeier equation for the SiO_2-clad material and with the measured refractive-index profile of the a-Si:H core. Then, from the spectral profiles of the effective group indices, the CD values of the waveguides were calculated, and compared with experimentally measured CD values using a white-light interferometric method.

The three different waveguides, all with 6-mm-long length and with tapered ends on both sides, were also used for measurement of the FWM-beam-generation efficiency with a fixed pump-wavelength of 1532 nm but with varying the signal-wavelength in the range from 1520 to 1570 nm. Among the three different waveguides of 400-, 450- and 500-nm widths, the FWM efficiency and the wavelength range of the efficient FWM conversion were the maximum for the 220-nm×450-nm a-Si:H waveguide because its zero CD wavelength was close to the pump wavelength.

Based on these results we could conclude that the CD profile of the amorphous silicon waveguide plays a critical role to the wide wavelength-range for an efficient FWM process compared to the pump power. The maximum FWM-efficiency of the waveguide was -35 dB for the coupled pump-power of +13 dBm, and the FWM-conversion wavelength-range was about 75 nm. Our devices used in this research were not optimized for low coupling and insertion losses. Further improvement on the FWM-efficiency in a-Si:H waveguides could be possible by having a low-loss characteristics of the waveguides through optimization of the device fabrication processes.

ACKNOWLEDGMENT

This work was supported in part by the Basic Science Research Programs through the National Research Foundation of Korea funded by the Korean Ministry of Education, Science and Technology under a Grant 2009-0084514 and by the Korean Ministry of Science, ICT & Future Planning under a Grant 2013R1A1A2012409.

REFERENCES

1. K. Y. Wang and A. C. Foster, "Ultralow power continuous-wave frequency conversion in hydrogenated amorphous silicon waveguides," Opt. Lett. **37**, 1331-1333 (2012).
2. B. Kuyken, S. Clemmen, S. K. Selvaraja, W. Bogaerts, D. V. Thourhout, P. Emplit, S. Massar, G. Roelkens, and R. Baets, "On-chip parametric amplification with 26.5 dB gain at telecommunication wavelengths using CMOS-compatible hydrogenated amorphous silicon waveguides," Opt. Lett. **36**, 552-555 (2011).
3. S. Suda, K. Tanizawa, Y. Sakakibara, T. Kamei, K. Nakanishi, E. Itoga, T. Ogasawara, R. Takei, H. Kawashima, S. Namiki, M. Mori, T. Hasama, and H. Ishikawa, "Pattern-effect-free all-optical wavelength conversion using a hydrogenated amorphous silicon waveguide with ultra-fast carrier decay," Opt. Lett. **37**, 1382-1384 (2012).
4. S. K. Selvaraja, E. Sleeckx, M. Schaekers, W. Bogaerts, D. V. Thourhout, P. Dumon, and R. Baets, "Low-loss amorphous silicon-on-insulator technology for photonic integrated circuitry," Opt. Commun. **282**, 1767-1770 (2009).
5. S. Zhu, G. Q. Lo, and D. L. Kwong, "Low-loss amorphous silicon wire waveguide for integrated photonics: effect of fabrication process and the thermal stability," Opt. Express **18**, 25283-25291 (2010).
6. M. A. Foster, A. C. Turner, J. E. Sharping, B. S. Schmidt, M. Lipson, and A. L. Gaeta, "Broad-band optical parametric gain on a silicon photonic chip," Nature **441**, 960-963 (2006).
7. A. C. Turner, C. Manolatou, B. S. Schmidt, M. Lipson, M. A. Foster, J. E. Sharping, and A. L. Gaeta, "Tailored anomalous group-velocity dispersion in silicon channel waveguides," Opt. Express **14**, 4357-4362 (2006).
8. R. M. Osgood Jr., N. C. Panoiu, J. I. Dadap, X. Liu, X. Chen, I.-W. Hsieh, E. Dulkeith, W. M. J. Green, and Y. A. Vlasov, "Engineering nonlinearities in nanoscale optical systems: physics and applications in dispersion-engineered silicon nanophotonic wires," Adv. in Opt. and Photon. **1**, 162-235 (2009).
9. D. Dimitropoulos, V. Raghunathan, R. Claps, and B. Jalali, "Phase-matching and nonlinear optical processes in silicon waveguides," Opt. Express **12**, 149-160 (2004).
10. J. E. Sharping, K. F. Lee, M. A. Foster, A. C. Turner, B. S. Schmidt, M. Lipson, A. L. Gaeta, and P. Kumar, "Generation of correlated photons in nanoscale silicon waveguides," Opt. Express **14**, 12388-12393 (2006).
11. D. W. Kim, S. H. Km, S. H. Lee, K. H. Kim, J.-M. Lee, and E.-H. Lee, "A new method of measuring localized chromatic dispersion of structured nanowaveguide devices using white-light interferometry," J. Lightwave Technol. **30**, 43-48 (2012).
12. N. Ophir, J. Chan, K. Padmaraju, A. Biberman, A. C.

Foster, M. A. Foster, M. Lipson, A. L. Gaeta, and K. Bergman, "Continuous wavelength conversion of 40-Gb/s data over 100 nm using a dispersion-engineered silicon waveguide," IEEE Photon. Technol. Lett. **23**, 73-75 (2011).
13. http://refractiveindex.info/?group=CRYSTALS&material=a-Si (SOPRA: Amorphous silicon 1).
14. R. J. Severens, G. J. H. Brussaard, M. C. M. van de Sander, and D. C. Schram, "Characterization of plasma beam deposited amorphous hydrogenated silicon," Appl. Phys. Lett. **67**, 491-493 (1995).
15. K. Okamoto, *Fundamentals of Optical Waveguides*, 2nd ed. (Elsevier, London, UK, 2006).
16. E. Dulkeith, F. Xia, L. Schares, W. M. J. Green, and Y. A. Vlasov, "Group index and group velocity dispersion in silicon-on-insulator photonic wires," Opt. Express **14**, 3853-3863 (2006).
17. Y. A. Vlasov, M. O'Boyle, H. F. Hamann, and S. J. McNab, "Active control of slow light on a chip with photonic crystal waveguides," Nature **438**, 65-69 (2005).
18. K. Inoue and T. Mukai, "Signal wavelength dependence of gain saturation in a fiber optical parametric amplifier," Opt. Lett. **26**, 10-21 (2001).
19. H.-S. Jeong, D. W. Kim, K. H. Kim, and J. Lee, "All-optical signal-conversion efficiency with parameter-dependent four-wave-mixing process in silicon nanowaveguide," J. Korean Phys. Soc. **62**, 428-434 (2013).
20. K. Narayanan and S. F. Preble, "Optical nonlinearities in hydrogenated-amorphous silicon waveguides," Opt. Express **18**, 8998-9005 (2010).
21. Y. Shoji, T. Ogasawara, T. Kamei, Y. Sakakibara, S. Suda, K. Kintaka, H. Kawashima, M. Okano, T. Hasama, H. Ishikawa, and M. Mori, "Ultrafast nonlinear effects in hydrogenated amorphous silicon wire waveguide," Opt. Express **18**, 5668-5673 (2010).